Astrophysics and Space Science manuscript No.
(will be inserted by the editor)

M. E. Gonzalez, V. M. Kaspi, F. Camilo, B. M. Gaensler and M. J. Pivovaroff

PSR J1119–6127 and the X-ray Emission from High Magnetic Field Radio Pulsars

Received: date / Accepted: date

Abstract The existence of radio pulsars having inferred magnetic fields in the magnetar regime suggests that possible transition objects could be found in the radio pulsar population. The discovery of such an object would contribute greatly to our understanding of neutron star physics. Here we report on unusual X-ray emission detected from the radio pulsar PSR J1119–6127 using XMM–Newton. The pulsar has a characteristic age of 1,700 yrs and inferred surface dipole magnetic field strength of 4.1×10^{13} G. In the 0.5-2.0 keV range, the emission shows a single, narrow pulse with an unusually high pulsed fraction of ∼70%. No pulsations are detected in the 2.0–10.0 keV range, where we derive an upper limit at the 99% level for the pulsed fraction of 28%. The pulsed emission is well described by a thermal blackbody model with a high temperature of $\sim2.4\times10^{6}$ K. While no unambiguous signature of magnetar-like emission has been found in high-magnetic-field radio pulsars, the X-ray characteristics of PSR J1119–6127 require alternate models from those of conventional thermal emission from neutron stars. In addition, PSR J1119–6127 is now the radio pulsar with the smallest characteristic age from which thermal X-ray emission has been detected.

Keywords ISM: individual (G292.2–0.5) · Pulsars: individual (PSR J1119–6127) · X-rays: ISM

PACS 97.60.Jd · 95.85.Nv · 97.60.Gb

M. E. Gonzalez and V. M. Kaspi
Department of Physics, Rutherford Physics Building, McGill University, Montreal, QC H3A 2T8, Canada. E-mail: gonzalez@physics.mcgill.ca

F. Camilo
Columbia Astrophysics Laboratory, Columbia University, 550 West 120th Street, New York, NY 10027, USA.

B. M. Gaensler
Harvard-Smithsonian Centre for Astrophysics, 60 Garden Street, Cambridge, MA 02138, USA; Current address: School of Physics, The University of Sydney, NSW 2006, Australia.

M. J. Pivovaroff
Lawrence Livermore National Laboratory, P.O. Box 808, L-258, Livermore, CA 94550, USA.

1 Introduction

The emission from the ∼1,500 radio pulsars (PSRs) discovered to date is generally thought to be powered by the loss of rotational kinetic energy due to magnetic braking. Radio pulsars with implied magnetic fields in the range $\sim10^{13-14}$ G have now been discovered, showing that radio emission can be produced in neutron stars with fields above the quantum critical field $B_c = 4.4\times10^{13}$ G. More exotic neutron stars with magnetic fields in the range $\sim10^{14-15}$ G have been observed at high energies and are believed to be powered by the decay of their large magnetic fields. Anomalous X-ray pulsars (AXPs) and Soft-Gamma Repeaters (SGRs) make up this class of so-called "magnetars" (Woods & Thompson 2004). As the inferred magnetic field strengths of radio pulsars and magnetars are now found to overlap, the underlying physical reasons for the differences in their emission properties remains a puzzle. To date, no radio pulsar has been observed to exhibit magnetar-like emission at high energies, posing an interesting challenge to current emission theories.

Here we summarize the analysis and results obtained from an XMM–Newton observations of PSR J1119–6127, originally published by Gonzalez et al. (2005). PSR J1119–6127 is one of the youngest radio pulsars known and also has one the highest inferred magnetic fields in the radio pulsar population. Our observation reveals unusual thermal emission from this object which may represent the first evidence for high-magnetic-field effects in the emission from a "normal" radio pulsar. We discuss these results in light of recent theoretical work on emission from highly magnetized neutron stars and observations of similar sources.

PSR J1119–6127, with spin period $P = 0.408$ s, is among the youngest radio pulsars known (Camilo et al. 2000). The measured braking index for the pulsar of $n = 2.91\pm0.05$ ($\dot{\nu} \propto -\nu^n$) implies an upper limit for the age of 1,700 yr. The pulsar has spin-down luminosity $\dot{E} \equiv 4\pi^2 I\dot{P}/P^3 = 2.3\times10^{36}$ erg s^{-1} (for a mo-

ment of inertia $I = 10^{45}$ g cm^2) and an inferred surface dipole magnetic field strength at the equator of $B \equiv 3.2\times10^{19}(P\dot{P})^{1/2}$ G $= 4.1\times10^{13}$ G. This value of B is among the highest known in the radio pulsar population. PSR J1119–6127 powers a small ($3''\times6''$) X-ray pulsar wind nebula (PWN, Gonzalez & Safi-Harb 2003), which results from the confinement of the pulsar's relativistic wind of particles and electromagnetic fields by the ambient medium . The pulsar lies close to the center of a $15'$-diameter "shell" supernova remnant (SNR), G292.2–0.5 (Crawford et al. 2001; Pivovaroff et al. 2001), located at a distance of 8.4±0.4 kpc, as determined from neutral hydrogen absorption measurements (Caswell et al. 2004).

2 Observation

We observed PSR J1119–6127 using the European Photon Imaging Camera (EPIC) aboard the XMM–Newton satellite on June 26, 2003. The MOS and PN instruments were operated in full-window and large-window mode, respectively. The temporal resolution was 2.6 s for MOS and 48 ms for PN. The data were analyzed using the Science Analysis System software (SAS v6.2.0) and standard reduction techniques. The effective exposure time was 48 ks for MOS1/MOS2 and 43 ks for PN.

Figure 1 shows the combined MOS image of the system in the 0.3–1.5 keV (*red*), 1.5–3.0 keV (*green*) and 3.0–10.0 keV (*blue*) bands[1]. The bright source at the center has coordinates $\alpha_{2000}=11^h19^m14.65^s$ and $\delta_{2000}=-61°27'50.2''$ ($4''$ error). This position coincides with the Chandra and radio coordinates of PSR J1119–6127. Although the spatial resolution of XMM–Newton (half power diameter of $15''$) permits the PWN to be neither resolved nor separated from the pulsar emission itself, XMM–Newton's sensitivity and high time resolution allow us to separate the pulsar's emission spectrally and temporally. The image reveals for the first time the detailed morphology of the SNR at X-ray energies as XMM–Newton's sensitivity was needed due to the remnant's low surface brightness. The large east-west asymmetry at low energies has been attributed to the presence of a molecular cloud on the east side of the field (Pivovaroff et al. 2001).

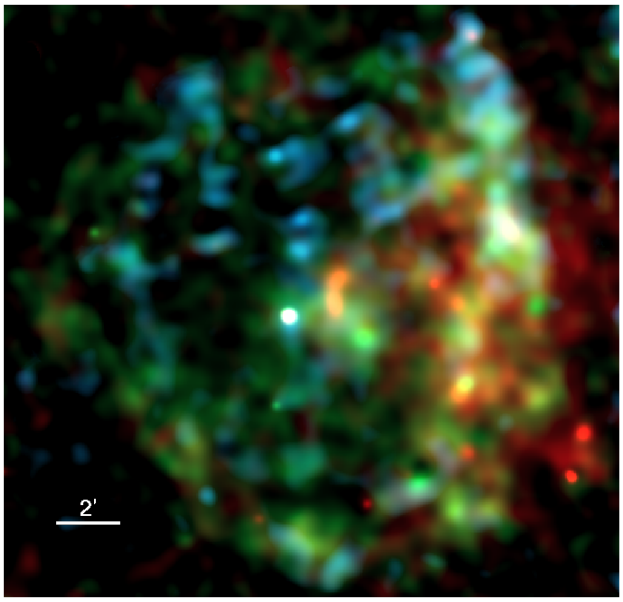

Fig. 1 Combined MOS image of G292.2–0.5 and PSR J1119–6127 in the 0.3–1.5 keV (*red*), 1.5–3.0 keV (*green*) and 3.0–10.0 keV (*blue*) bands. Individual MOS1/MOS2 images were first binned into pixels of $2.5''\times2.5''$ and unrelated point sources in the field were excluded. These images were then added and adaptively smoothed with a Gaussian with $\sigma=5''$–$15''$ to obtain signal-to-noise ratios higher than 3. Background images and exposure maps at each energy band were similarly obtained and used to correct the final images.

3 Results

3.1 Timing Analysis

The PN data were used to search for pulsations from PSR J1119–6127. A circular region of $25''$-radius centered at the X-ray coordinates of the pulsar was used to extract the source photons. The data were divided into different energy ranges at 0.5–10.0 keV (620±30 photons), 0.5–2.0 keV (340±25 photons) and 2.0–10.0 keV (275±22 photons). The most significant signal was detected in the 0.5–2.0 keV range with $Z_2^2 = 52.8$ (6.6σ significance) at a frequency of 2.449726(6) Hz (1σ errors). This frequency is in agreement with the radio prediction for PSR J1119–6127 obtained using regular monitoring with the Parkes telescope. In the 2.0–10.0 keV range, no signal was found with a significance $>2.8\sigma$. In the 0.5–10.0 keV range, the above signal was detected with a 5.2σ significance.

Figure 2 shows the resulting pulse profiles at 0.5–2.0 keV (top, left) and 2.0–10.0 keV (top, right). The background was estimated from a nearby region away from bright SNR knots. The horizontal dashed lines represent our estimates for the contribution from the pulsar's surroundings obtained using the Chandra observation of the pulsar (Gonzalez & Safi-Harb 2003). The Chandra count rate excluding the pulsar was used to estimate the XMM–Newton counts using *WebPIMMS*. The resulting pulsed fraction [PF $\equiv (F_{max}–F_{min})$ / $(F_{max}+F_{min})$] is labeled in Figure 2 (1σ statistical errors). In the 2.0–10.0 keV range, we derive an upper limit for the pulsed fraction of 28% (at the 99% confidence level; see, e.g., Vaughan et al. 1994; Ransom et al. 2002). The radio emission from PSR J1119–6127 consists of a single peak of duty cycle 5% and luminosity at 1.4 GHz of 28 mJy kpc^2 (Camilo et al. 2000). Phase zero in the X-ray profiles cor-

[1] The detailed spatial distribution in the 3.0–10.0 keV (*blue*) image should be examined with caution as this energy band suffered from a high degree of stray-light contamination from a nearby high-energy source.

responds to the radio peak (determined with 3 ms uncertainty). Taking into account the low temporal resolution of the XMM–Newton observation (phase bin width of 51 ms), this result suggests that the radio peak is in phase with the X-ray peak within our uncertainties, or possibly just slightly ahead. Additional observations at higher temporal resolution will help to confirm and constrain these results.

3.2 Spectral Analysis

The EPIC data were used to perform a spectral analysis of PSR J1119–6127. Circular regions with radii of 20″ and 25″ were used for MOS and PN, encompassing ∼75% and ∼78% of the source photons, respectively. The derived fluxes have been corrected accordingly. Background regions were chosen from nearby areas away from bright SNR knots. The spectra were fit in the 0.5–10.0 keV range using XSPEC (v.11.3.0) with a minimum of 20 counts per bin from a total of 240±19, 210±18, and 620±30 background-subtracted counts in MOS1, MOS2 and PN, respectively.

Two-component models were needed in order to describe the low and high energy portions of the spectra. A non-thermal power-law component with photon index $\Gamma \sim 1.5$ described the high-energy emission in the spectra well. In turn, various models were used to describe the low-energy emission. The derived fits are summarized in Table 1.

We also extracted PN spectra from the "pulsed" and "unpulsed" regions of the pulse profile, at phases 0.7–1.3 (430±28 counts) and 0.3–0.7 (200±20 counts), respectively. These spectra are shown in Figure 2 (bottom) and were well fit by two-component models that agree with those derived for the phase-averaged spectra. For example, a blackbody plus power-law model yielded $T^{\infty} = 2.8\pm0.4$ MK and $\Gamma = 1.4^{+0.5}_{-0.2}$ (1σ errors). The main difference between the pulsed and unpulsed spectra was found to be the relative contributions of the model components. The pulsed spectrum is dominated by the soft component below ∼2 keV, while the unpulsed spectrum is dominated by the hard, power-law component at all energies.

Table 1 Fits to the XMM–Newton phase-averaged spectrum of PSR J1119–6127

Parameter	PL+PL ($\pm1\sigma$)	BB+PL ($\pm1\sigma$)	Atm[a]+PL ($\pm1\sigma$)
N_H (10^{22} cm^{-2})	$2.3^{+0.4}_{-0.3}$	$1.6^{+0.4}_{-0.3}$	$1.9^{+0.5}_{-0.3}$
χ^2(dof)	79(66)	78(66)	78(66)
Soft component characteristics			
Γ or T^{∞}	6.5±0.9	$2.4^{+0.3}_{-0.2}$ MK	0.9±0.2 MK
R^{∞} (km)	...	$3.4^{+1.8}_{-0.3}$	12 (fixed)
d (kpc)	8.4 (fixed)	8.4 (fixed)	$1.6^{+0.2}_{-0.9}$
${f_{abs}}^b$ (10^{-14})	$2.1^{+2.3}_{-0.9}$	$1.5^{+1.8}_{-0.2}$	$1.7^{+7.0}_{-0.4}$
${f_{unabs}}^b$ (10^{-13})	63^{+57}_{-32}	$2.4^{+3.0}_{-0.5}$	$7.2^{+31}_{-1.6}$
${L_X}^b$ (10^{33})	53^{+50}_{-27}	$2.0^{+2.5}_{-0.4}$	$0.22^{+0.88}_{-0.05}$
Hard component characteristics			
Γ	$1.3^{+0.5}_{-0.2}$	$1.5^{+0.3}_{-0.2}$	$1.5^{+0.2}_{-0.3}$
${f_{abs}}^b$ (10^{-14})	$7.1^{+10}_{-1.5}$	$7.4^{+3.6}_{-1.0}$	$7.3^{+4.7}_{-2.7}$
${f_{unabs}}^b$ (10^{-13})	$1.0^{+1.6}_{-0.2}$	$1.1^{+0.6}_{-0.2}$	$1.1^{+0.8}_{-0.3}$
${L_X}^b$ (10^{33})	$0.8^{+1.3}_{-0.2}$	$0.9^{+0.5}_{-0.1}$	0.04±0.02

[a] The atmospheric model was computed with B=10^{13} G and pure hydrogen composition. The local values for the temperature, T, and radius, R = 10 km, of the star have been redshifted to infinity according to the formulae T^{∞}=$T(1–2GM/Rc^2)^{1/2}$ and R^{∞}=$R(1–2GM/Rc^2)^{-1/2}$, with M = 1.4 $M_{\odot}$.

[b] The 0.5–10.0 keV absorbed and unabsorbed fluxes, f_{abs} and f_{unabs}, have units of ergs s^{-1} cm^{-2}. The 0.5–10.0 keV X-ray luminosity, L_X, at the distance d, is in units of ergs s^{-1}.

4 Discussion

4.1 Observed Emission Characteristics

The pulse profile in the 0.5–2.0 keV range shows a single, narrow pulse with a high pulsed fraction. Modeled as a Gaussian, the full-width at half maximum is $0.26^{+0.08}_{-0.06}P$ (1σ errors) with χ^2(dof) = 2.1(4) and a probability of 0.72. A sinusoidal fit resulted in χ^2(dof) = 8.9(5) with a probability of 0.11. Due to the limited statistics available, the Gaussian fit is preferred only at the 2.4σ level (according to the F-test). A two-component profile cannot be ruled out with the present data (e.g., sine curve plus a narrow peak, or two narrow peaks at phases ∼0.8 and ∼1.1). Additional X-ray observations at higher temporal resolution are needed to further constrain the pulse shape.

The observed spectrum from PSR J1119–6127 requires two-component models. The hard, non-thermal component is consistent with arising from the pulsar's surroundings. Using the high-resolution Chandra data we estimate that the PWN plus SNR emission within a 25″ radius, excluding the pulsar, is well described by a power-law model with Γ=$1.8^{+0.8}_{-0.6}$ and unabsorbed flux in the 0.5–10.0 keV range of $0.9^{+0.6}_{-0.5}\times10^{-13}$ erg s^{-1} cm^{-2} (1σ errors). These values are in good agreement with the hard power-law component shown in Table 1. Although a small contribution from the pulsar to this hard emission cannot be ruled out, it would not affect our results on the pulsar's soft emission.

The soft spectral component must then arise from the pulsar. Non-thermal X-ray spectra from radio pulsars have photon indices in the range $0.5<\Gamma<2.7$ (Becker & Aschenbach 2002; Pavlov et al. 2002). Models for synchrotron emission in the pulsar magnetosphere(Cheng & Zhang 1999; Rudak & Dyks 1999) predict $\Gamma \lesssim 2$. The pulsed emission we detect from PSR J1119–6127, if interpreted as non-

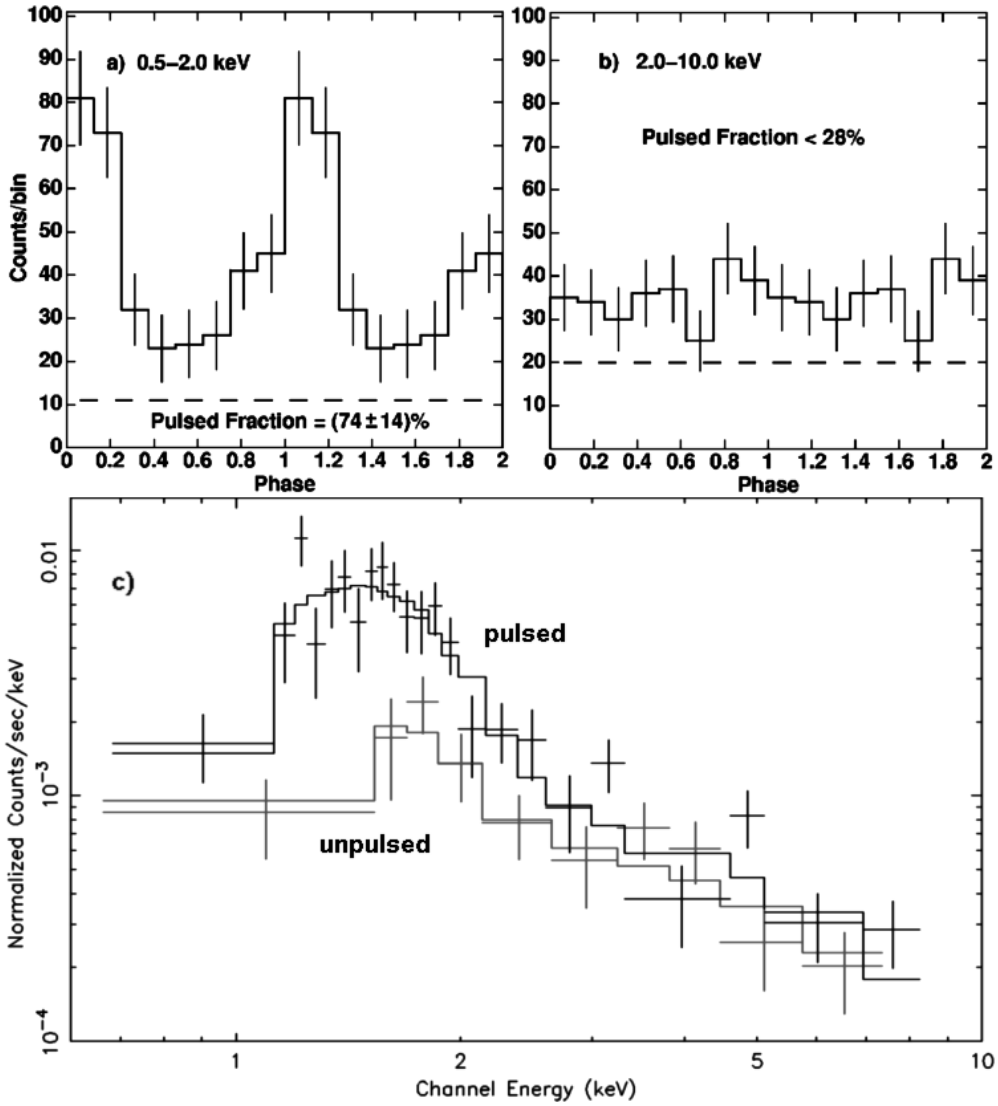

Fig. 2 *Top*: X-ray pulse profiles of PSR PSR J1119–6127 in the 0.5–2.0 keV (*left*) and 2.0–10.0 keV (*right*) ranges. Errors bars are 1σ and two cycles are shown. The dashed lines represent our estimates for the contribution from the pulsar's surroundings (see §3.1). *Bottom*: EPIC-PN spectra obtained for the pulsed (*black*) and unpulsed (*red*) regions of the pulse profile with their respective best-fit blackbody plus power-law model (solid curves).

thermal in origin, has a steeper spectrum (Γ=6.5±0.9, Table 1) than those observed or predicted. Therefore, a thermal origin for the observed emission is strongly favored with the present data. In addition, atmospheric models require small distances (or conversely, implausibly large emitting radii at 8.4 kpc) to account for the observed emission. We therefore favor a blackbody model to account for the observed emission.

The blackbody temperature of the X-ray emission from PSR J1119–6127 is $T_{bb}^{\infty} = (2.4^{+0.3}_{-0.2})\times10^6$ K. This temperature is among the highest seen in radio pulsars; while it is naively similar to those found in much older pulsars, none of them exhibits a higher temperature at statistically significant levels (e.g., PSR J0218+4232 has a characteristic age of $\tau_c = P/2\dot{P} = 5.1\times10^8$ yr and a blackbody temperature of $T_{bb}^{\infty} = 2.9\pm1.1\ \times10^6$ K, 3σ errors, Webb et al. 2004). PSR J1119–6127 is now the youngest radio pulsar from which thermal emission has been detected, the next youngest being Vela (τ_c = 11 kyr) with a blackbody temperature $T_{bb}^{\infty} = (1.47\pm0.18)\times10^6$ K (3σ range, Pavlov et al. 2001). Moreover, the pulsed fraction of the thermal emission from PSR J1119–6127 is significantly higher than is seen in other radio pulsars; thermal sources where the emission arises from the entire surface or for localized regions show pulsed fractions at low energies of $\lesssim$40% (Pavlov et al. 2001, 2002; Becker & Aschenbach 2002). The narrow peak in the pulse profile points to yet another difference from what is normally seen in thermal emission from radio pulsars at

Table 2 High-Magnetic Field Radio Pulsars

PSR	J1847–0130	J1718–3718	J1814–1744	J1846–0258	B0154–61	B1509–58
P (sec)	6.7	3.4	4	0.32	2.35	0.15
B (10^{13} G)	9.4	7.4	5.5	4.8	2.1	1.5
τ_c (kyr)	83	34	85	0.72	197	1.7
$\dot{E}$ (ergs s^{-1})	1.7×10^{32}	1.5×10^{33}	4.7×10^{32}	8×10^{36}	5.7×10^{32}	1.8×10^{37}
D (kpc)	$\sim$8	4–5	$\sim$10	$\sim$19	$\sim$1.7	$\sim$5
L_X (ergs s^{-1})	$<5\times10^{33}$	$\sim10^{30}$	$<6\times10^{35}$	6.4×10^{34}	$<1.4\times10^{32}$	2.4×10^{34}
T or Γ	–	$T\sim$1.6 MK	–	$\Gamma\sim$1.4	–	$\Gamma\sim$1.4
Ref.	McLaughlin et al. (2003)	Kaspi & McLaughlin (2005)	Pivovaroff et al. (2000)	Helfand et al. (2003)	Gonzalez et al. (2004)	Gaensler et al. (2002)

low energies (Pavlov et al. 2002; Becker & Aschenbach 2002), namely broad pulsations.

4.2 Thermal Emission Mechanisms

Conventional models for thermal emission from neutron stars cannot account for the observed characteristics in PSR J1119–6127. Thermal emission from polar-cap reheating has been well studied and, whether the required return currents arrive from the outer gap region (Cheng & Zhang 1999) or from close to the polar cap (Harding & Muslimov 2001), the X-ray luminosity is constrained to be $\lesssim10^{-5}\dot{E}$ for sources as young as PSR J1119–6127. This is at least 2 orders of magnitude below what we observe.

Thermal emission may also arise from the surface due to initial cooling. The observed luminosity is consistent with predictions from standard models of cooling neutron stars (Yakovlev et al. 2004; Page et al. 2005). However, the effective blackbody temperature is higher than predicted and the observed blackbody radius is smaller than allowed from neutron star equations of state (Lattimer & Prakash 2000). The very high observed pulsed fraction is also consistent with emission arising from a small fraction of the neutron star surface.

On the other hand, recent work on surface emission from highly magnetized neutron stars has explored the effects of a high magnetic field, as heat conductivity is expected to be suppressed perpendicular to the field lines and will be channeled along the lines instead (Geppert et al. 2004; Pérez-Azorín et al. 2006a). This will produce a highly anisotropic temperature distribution on the surface of the star, with small, hot regions at the magnetic poles. Highly modulated thermal emission with high temperatures will then be produced. These results have been applied to model the observed emission from RXJ 0720.4–3125, a highly magnetized neutron star, with apparent success (Perez-Azorin et al. 2006b). Pulsed fractions as high as $\sim$30% in the case of isotropic blackbody emission have been reported (Geppert et al. 2005). Therefore, it remains to be shown whether the same models can be applied to reproduce the observed emission characteristics in PSR J1119–6127. In this case, PSR J1119–6127 would be the first radio pulsar to show the effects of a high magnetic field through its X-ray emission.

We also point out the thermal emission with high temperature and high pulsed fraction that was found for PSR J1852+0040 (Gotthelf et al. 2005). Although a detailed timing solution has not been reported, initial estimates suggest a characteristic age of $\tau_c > 24$ kyr and low magnetic field of $B < 3\times10^{12}$ G. If these estimates are correct, existing theories for thermal emission from neutron stars cannot readily account for the observed characteristics, including those involving high-magnetic-field effects as mentioned above.

4.3 Other High-Magnetic Field Pulsars

Many radio pulsars having inferred magnetic fields in the range 10^{13-14} G have now been discovered. A sample of these pulsars with associated X-ray observations is shown in Table 2. Most of these sources have proved to be very faint in X-rays. Only two pulsars, PSRs J1846–0258 and B1509–58, are bright non-thermal sources and power bright PWNe. As expected, and in agreement with normal radio pulsars, they are young and very energetic ($\tau_c < 2{,}000$ yrs and $\dot{E} > 10^{36}$ ergs s^{-1}).

On the other hand, the older and less energetic pulsars in Table 2 have not been detected in X-rays ($\tau_c > 10{,}000$ yrs and $\dot{E} < 10^{33}$ ergs s^{-1}). This includes PSR J1847–0130, the radio pulsar with highest inferred magnetic field discovered to date (0.9×10^{14} G). These pulsars then show no enhancement of high-energy emission despite having inferred magnetic fields in the magnetar range. One intermediate case is that of PSR J1718–3718, which does have a faint X-ray counterpart seen with Chandra. However, the detailed characteristics of this emission (e.g., thermal vs. non-thermal) could not be constrained with the data.

PSR J1119–6127 is then an interesting and puzzling source. Despite being young and energetic, it does not power a bright PWN and we have found its emission to be dominated by a thermal component. This is in direct contrast to the sources mentioned above, particularly PSR J1846–0258 with which PSR J1119–6127 shares almost identical spin characteristics and even similar surroundings in their respective SNRs (Helfand et al. 2003; Gonzalez & Safi-Harb 2005). It is therefore unclear what

the physical reasons are behind their vastly different X-ray emission. In addition, while it is possible that the characteristics observed in PSR J1119–6127 may be due to heat conductivity effects on a highly magnetized atmosphere, the emission is not magnetar-like.

5 Conclusion

The X-ray emission from the young, high magnetic field radio pulsar PSR J1119–6127 shows a thermal spectrum with high temperature and small emitting radius, making it the radio pulsar with smallest characteristic age from which thermal X-ray emission has been detected. The pulse profile of this emission is consistent with a single, narrow pulse with a high pulsed fraction. Hot spots heated by back-flowing particles from the magnetosphere are not expected in such a young source, while the X-ray characteristics are not consistent with cooling emission from the whole surface. However, a highly anisotropic temperature distribution on the surface due to a high magnetic field may be able to account for the observed characteristics. This would make PSR J1119–6127 the first radio pulsar to exhibit high-magnetic-field effects on its X-ray emission. Additional X-ray observations, particularly with improved temporal resolution, will help to confirm and constrain the observed characteristics.

Many high magnetic field radio pulsars have now been observed in X-rays, some with very similar spin characteristics to PSR J1119–6127 and others with higher inferred fields, but it remains unclear why PSR J1119–6127 is to date the only one to show such effects. Recently, the discovery of radio emission from a magnetar (Camilo et al. 2006) has shown that such emission is possible in these sources, contributing to our understanding of the mechanisms at work. However, we still lack an understanding for the absence of magnetar-like emission from radio pulsars with high magnetic fields and additional observations of these objects are then needed.

References

Becker, W., & Aschenbach, B., in Proc. 270th WE-Heraeus Seminar on Neutron Stars, Pulsars, and Supernova Remnants, ed. W. Becker, H. Lesch, & J. Trümper (MPE Rep. 278; Garching: MPE), 64 (2002) (astro-ph/0208466)

Camilo, F., Kaspi, V. M., Lyne, A. G. et al. ApJ, **541**, 367 (2000)

Camilo, F., Ransom, S., Halpern, J. et al. Nature, in press (2006) (astro-ph/0605429)

Caswell, J. L., McClure-Griffiths, N. M., & Cheung, M. C. M., MNRAS, **352**, 1405 (2004)

Cheng, K. S., & Zhang, L., ApJ, **515**, 337 (1999)

Crawford, F., Gaensler, B. M., Kaspi, V. M. et al. ApJ, **554**, 152 (2001)

Gaensler, B. M., Arons, J., Kaspi, V. M. et al. ApJ, **569**, 878 (2002)

Geppert, U., Kueker, M., & Page, D., ArXiv Astrophysics e-prints (2005), astro-ph/0512530

Geppert, U., Küker, M., & Page, D., A&A, **426**, 267 (2004)

Gonzalez, M., & Safi-Harb, S., ApJ, **591**, L143 (2003)

Gonzalez, M., & Safi-Harb, S., ApJ, **619**, 856 (2005)

Gonzalez, M. E., Kaspi, V. M., Camilo, F. et al. ApJ, **630**, 489 (2005)

Gonzalez, M. E., Kaspi, V. M., Lyne, A. G. et al. ApJ, **610**, L37 (2004)

Gotthelf, E. V., Halpern, J., Seward, F. D. ApJ, **627**, 390 (2005)

Harding, A. K., & Muslimov, A. G., ApJ, **556**, 987 (2001)

Helfand, D. J., Collins, B. F., & Gotthelf, E. V., ApJ, **582**, 783 (2003)

Kaspi, V. M., & McLaughlin, M. A., ApJ, **518**, 41 (2005)

Lattimer, J. M., & Prakash, M., PhR, **333**, 121 (2000)

McLaughlin, M. A., Stairs, I. H., Kaspi, V. M. et al. ApJ, **591**, L135 (2003)

Page, D., Geppert, U., & Weber, F., to be published in Nucl. Phys. A (2005) (astro-ph/0508056)

Pavlov, G. G., Zavlin, V. E., & Sanwal, D., in Proc. 270th WE-Heraeus Seminar on Neutron Stars, Pulsars, and Supernova Remnants, ed. W. Becker, H. Lesch, & J. Trümper (MPE Rep. 278; Garching: MPE), 273 (2002) (astro-ph/0206024)

Pavlov, G. G., Zavlin, V. E., Sanwal, D. et al. ApJ, **552**, L129 (2001)

Pérez-Azorín, J. F., Miralles, J. A., & Pons, J. A., A&A, **451**, 1009 (2006a)

Perez-Azorin, J. F., Pons, J. A., Miralles, J. A. et al. ApJ, submitted (2006b) (astro-ph/0603752)

Pivovaroff, M., Kaspi, V. M., & Camilo, F., ApJ, **535**, 379 (2000)

Pivovaroff, M. J., Kaspi, V. M., Camilo, F. et al. ApJ, **554**, 161 (2001)

Ransom, S. M., Eikenberry, S. S., & Middleditch, J., AJ, **124**, 1788 (2002)

Rudak, B., & Dyks, J., MNRAS, **303**, 477 (1999)

Vaughan, B. A., van der Klis, M., Wood, K. S. et al. ApJ, **435**, 362 (1994)

Webb, N. A., Olive, J.-F., & Barret, D., A&A, **417**, 181 (2004)

Woods, P. M., & Thompson, C., in Compact Stellar X-ray Sources, ed. W. H. G. Lewin & M. van der Klis (UK: Cambridge University Press), in press (2004) (astro-ph/0406133)

Yakovlev, D. G., Gnedin, O. Y., Kaminker, A. D. et al. Advances in Space Research, **33**, 523 (2004)